EIGHTH EUROPEAN ROTORCRAFT FORUM

Paper No. 2.10

A LIFTING LINE THEORY FOR CURVED HELICOPTER BLADES IN HOVERING AND AXIAL FLIGHT

O. RAND and A. ROSEN

Department of Aeronautical Engineering
Technion - Israel Institute of Technology
Haifa, Israel

August 31 through September 3, 1982

AIX-EN-PROVENCE, FRANCE

ASSOCIATION AERONAUTIQUE ET ASTRONAUTIQUE DE FRANCE

A Lifting Line Theory for Curved Helicopter Blades in Hovering and Axial Flight

O. Rand and A. Rosen

Department of Aeronautical Engineering
Technion - Israel Institute of Technology
Haifa, Israel

Abstract

A lifting line model to calculate the aerodynamic loads along a curved helicopter blade, in hovering and axial flight, is derived. In the derivation a "semi-rigid" wake model, which depends on the induced velocity distribution along the blade, is used. The influence of both, trailing and bound vortices, are taken into account. The derivation yields an efficient numerical scheme of calculations. Results for two different curved blades are presented and compared with similar straight blades. It is shown that curvature influences the distribution of the aerodynamic properties along the blades. Good agreement between the results of the present lifting line theory and a "momentum-blade element" theory for curved blades is also presented.

1. Introduction

At the beginning helicopter rotors included only straight blades. During recent years increasing numbers of rotors have blades with swept tips. These swept tips have a significant influence on the aerodynamic, structural and aeroelastic behavior of these blades as can be seen for example in [1] and many other references. In existing rotors usually only less than ten percent of the blade's tip are swept back although investigation of cases where 35 of the blade is swept back has also been reported [2]. It seems that because of the beneficial effects most of the helicopter blades in the future will not be straight.

In a recent research [3] the authors of the present paper investigated the aeroelastic behavior of helicopter blades which are not straight, namely curved blades, during hovering and axial flight. In that research, in order to calculate the aerodynamic loads, the well known "momentum-blade element" theory has been extended to also include curved blades. The purpose of the present paper is to develop a lifting line model which is capable of calculating the aerodynamic loads along curved blades of a helicopter in hovering and axial flight. This model will be used in order to calculate the load distribution along blades having different geometries. The results of the lifting line model will be compared with the results which are obtained by using the "momentum-blade element" theory.

The derivation of the present paper follows similar path to the derivation which has been presented in [4] for straight blades.

2. Theoretical Derivation

2.1 General Description

The present paper deals with a helicopter rotor having b identical, equally spaced, blades. These blades rotate about the shaft with a constant rotational velocity Ω and the rotor hovers or is in axial flight (in the direction of the shaft).

In order to solve the problem, the blades are presented by curved lifting lines. The circulation along the lifting line is denoted by Γ. Since generally Γ varies along the blade, vortex filaments trail behind the rotating blade. It is assumed that each vortex element which leaves the blade moves downward with a velocity which is equal to the sum of the rotor axial velocity and the induced velocity at the point where this element departs from the blade. Using this model one is faced with a problem which doesn't arise in the case of straight blades. The problem is that in the case of curved blades the vortex lines are not perpendicular to the lifting line at the point of departure. This results in infinite induced velocities along the lifting line. This problem also appears in the case where one tries to apply the lifting line theory to swept or curved wings of fixed-wing aircraft or to helicopter rotors (with straight blades) in the case of forward flight. Discussion of this problem appears for example in [5] or [6]. It seems that the problem can be overcome if one recalls that the lifting line theory is a combination of exterior solution of the velocity which is induced on a certain point of the lifting line by the whole wake field and the rest of the lifting line- and an interior solution associated with the two-dimensional airfoil theory. Exact representation of the interior solution includes a distribution of two-dimensional vortices along the blade chord. If such representation is employed the physical difficulties are removed. More details may be found in [5, 6]. Another problem which is raised in the case of curved blades is the fact that also the velocity which is induced on the lifting line by the bound vortex itself, obtains infinite values (see also [7]). This problem is solved by the same argument which was given above concerning the trailing vortex lines. Although the problems of an infinite induced velocity are of an important physical nature, they do not impose any practical difficulty since they are automatically overcome when the discrete model which will be described in what follows, is used. In this model the blade is replaced by straight elements with a control point at the middle of each. Thus the induced velocities at the control points become finite.

2.2 The Lifting Line and Wake Model

As pointed out before, each blade is replaced by a lifting line which passes at the forward quarter chord of each cross section. Figure 1 presents the projection of the blade geometry on the hub plane which is defined by the coordinate lines x_{HUB} and y_{HUB}. The coordinate z_{HUB} coincides with the shaft. e is the offset of the rotor, x_c is the root cut out while R is the radius of the rotor. The lifting line is divided into m elements by the points $\eta_1, \eta_2 \ldots \eta_{m+1}$. Each of these points is defined by its radial

distance from the origin of the coordinates x_{HUB}, y_{HUB}. These radial distances equal $R\eta_1$, $R\eta_2$....etc. It should be emphasized that the division is usually not uniform while a more refined division exists towards the blade tip, where most of the loads are concentrated and in regions where the curvature or changes of curvature are significant.

Now the curved lifting line is replaced by straight segments connecting the point η_1, η_2....η_{m+1} (see Fig. 1). At the middle of each such straight element a control point is defined. These control points x_1, x_2....x_m are characterized by their radial distances Rx_1, Rx_2....Rx_m respectively. The following relation therefore exists:

$$x_i = (\eta_i + \eta_{i+1})/2 \tag{1}$$

It is assumed that the circulation between the division points is constant and changes in the circulation occurs only while passing from one segment to its neighbour. Based on this assumption any segment j becomes associated with a horseshoe vortex which is composed of the segment of the lifting line between the points η_j and η_{j+1}, and the two free vortices trailing from these points. The circulation of this horseshoe vortex equals Γ_j.

At this point a semi rigid wake model which determines the path of the trailing vortices is adopted. This model is based on the following two assumptions:

a) Flapping and elastic displacements of the blades are neglected and its is assumed that the blades remain straight and lie in the HUB plane.

b) Each element of the trailing vortices which spring from the blade moves in space in a rectilinear motion, parallel to the z_{HUB} direction.

The velocity of the motion of the element along the line is constant and equal to the sum of the axial velocity of the rotor and the axial component (in the $-z_{HUB}$ direction) of the induced velocity. This assumption means that contraction of the wake, which should be important in the case of heavily loaded rotors, is neglected and the induced tangential velocity is negligible compared to the blade rotational speed.

According to the above assumptions each vortex line which leaves the blade and belongs to the j^{th} horseshoe vortex moves in the $-z_{HUB}$ direction with a velocity v'_j which is given by:

$$v'_j = V_c + v_j \tag{2}$$

where v_j is the induced velocity at the j^{th} control point and V_c the axial velocity of the rotor. Thus a typical trailing wake, composed of helical vortex lines, is obtained.

2.3 Calculating the Induced Velocities

In Fig. 2 two segments of the curved blade, the i^{th} and j^{th} segments, are shown. The purpose of this subsection is to calculate the velocity which is induced by the j^{th} horseshoe vortex, at the control point x_i. For the sake of simplicity it is initially assumed that the circulation of the j^{th} horseshoe is of unit intensity. It should be remembered that the rotor has b equally spaced blades. Therefore, in addition to the j^{th} element which belongs to the same blade as the control point x_i and which angle is ϕ_j (ϕ_j is measured to the control point x_j as shown in Fig. 2), there are other (b-1) j^{th} elements the locations of which are: $(\phi_j + 2\pi/b)$, $(\phi_j + 4\pi/b)\ldots[\phi_j + (b-1)2\pi/b]$. Expressions for the velocity which is induced in the disc plane by b equally spaced helical vortex lines are well known and could be found for example in [4,5]. It is found that the velocity in the $-z_{HUB}$ direction, which is induced at the control point x_i by all the vortex lines which leave the b blades at the point n_j, equals:

$$v_{fi,j} = -\frac{1}{4\pi R}\sum_{n=1}^{b}\int_0^{\infty}\frac{n_j^2 - n_j x_i \cos(\tilde{\theta}_{n,j} - \nu - \psi)}{[\tilde{v}'^2_j \nu^2 + n_j^2 + x_i^2 - 2n_j x_j \cos(\tilde{\theta}_{n,j} - \nu - \psi)]^{3/2}}\,d\nu \qquad (3)$$

where:

$$\tilde{\theta}_{n,j} = \tilde{\theta}_j + \gamma_n \qquad (\tilde{\theta}_j \text{ is defined in Fig. 2}) \qquad (4)$$

and:

$$\gamma_n = \frac{2\pi}{b}(n-1) \qquad n = 1,2,\ldots b \qquad (5)$$

$\tilde{v}'_j$ is a nondimensional velocity which is obtained after v'_j is divided by ΩR. Similarily the axial velocity which is induced at the same control point by all the vortex lines which leave the b blades at the point n_{j+1}, equals:

$$v_{fi,j+1} = \frac{1}{4\pi R}\sum_{n=1}^{b}\int_0^{\infty}\frac{n_{j+1}^2 - n_{j+1} x_i \cos(\tilde{\theta}_{n,j+1} - \nu - \psi)}{[\tilde{v}'^2_j \nu^2 + n_{j+1}^2 + x_i^2 - 2n_{j+1} x_i \cos(\tilde{\theta}_{n,j+1} - \nu - \psi)]^{3/2}}\,d\nu \qquad (6)$$

where:

$$\tilde{\theta}_{n,j+1} = \tilde{\theta}_{j+1} + \gamma_n \qquad (7)$$

From Fig. (2) it turns out that:

$$\tilde{\theta}_j = \psi + \alpha_{i,j} \qquad (8a) \qquad\qquad \tilde{\theta}_{j+1} = \psi + \alpha_{i,j+1} \qquad (8b)$$

Based on Eqs. (3) - (8) it is clear that the axial velocity which is induced at the control point x_i by the two vortex lines which are trailed from all the b j^{th} horseshoe vortices (of unity strength) equals:

$$VT_{ij} = \frac{1}{4\pi R}\left\{\int_{\alpha_{i,j+1}}^{\infty} P1_{ij}\,d\nu - \int_{-\alpha_{i,j}}^{\infty} P2_{ij}\,d\nu\right\} \qquad (9)$$

where:

$$P1_{ij} = \sum_{n=1}^{b} \frac{n_{j+1}^2 - n_{j+1}x_i\cos(x_n - \nu)}{[\tilde{v'}_j^2(\nu + \alpha_{i,j+1})^2 + n_{j+1}^2 + x_i^2 - 2n_{j+1}x_i\cos(\gamma_n - \nu)]^{3/2}} \qquad (10a)$$

$$P2_{ij} = \sum_{n=1}^{b} \frac{n_j^2 - n_j x_i\cos(\gamma_n - \nu)}{[\tilde{v'}_j^2(\nu + \alpha_{i,j})^2 + n_j^2 + x_i^2 - 2n_j x_i\cos(\gamma_n - \nu)]^{3/2}} \qquad (10b)$$

Since ν obtains very large values while $\alpha_{i,j}$ and $\alpha_{i,j+1}$ have finite values, it is clear that it is always possible to find ν_s, such that:

$$\alpha_{i,j}\ ,\ \alpha_{i,j+1} << \nu_s \qquad (11)$$

Based on Eq. (11), Eq. (9) can be approximated as:

$$VT_{ij} \cong \frac{1}{4\pi R}\left[\int_{-\alpha_{i,j+1}}^{\nu_s} P1_{ij}\,d\nu - \int_{-\alpha_{i,j}}^{\nu_s} P2_{ij}\,d\nu + \int_{\nu_s}^{\infty} P_{ij}\,d\nu\right] \qquad (12)$$

where:

$$P_{ij} = P1_{ij} - P2_{ij} \qquad for \qquad \alpha_{i,j} = \alpha_{i,j+1} = 0 \qquad (14)$$

In the case of straight blades:

$$\alpha_{i,j} = \alpha_{i,j+1} = \nu_s = 0 \qquad (15)$$

Then the first two integrals inside the square brackets of Eq. (12) disappear and VT_{ij} become equal to V_{ij} which are the influence coefficients in the case of straight blades and which have been presented and investigated very extensively in [4]. V_{ij} are defined as:

$$V_{ij} = \frac{1}{4\pi R}\int_0^{\infty} P_{ij}\,d\nu \qquad (16)$$

In [4] a very efficient technique of calculating and using V_{ij} has been derived and described. In order to use this technique, Eq. (12) is written as:

$$VT_{ij} \cong V_{ij} + C_{ij} \tag{17}$$

where:

$$C_{ij} = \frac{1}{4\pi R}\left[\int_{-\alpha_{i,j+1}}^{\nu_s} P1_{ij}d\nu - \int_{-\alpha_{i,j}}^{\nu_s} P2_{ij}d\nu - \int_{0}^{\nu_s} P_{ij}d\nu\right] \tag{18}$$

C_{ij} presents the corrections to the influence coefficients of the trailing wake due to the curvature of the blade. In all the cases of interest here, as those that will be presented in the examples, $\alpha_{i,j}$ and $\alpha_{i,j+1}$ are small angles. Moreover, in the most important cases of the influence of the horseshoe vortex on its own control point or the neighbour control point meaning j=i or j=i±1, $\alpha_{i,j}$ and $\alpha_{i,j+1}$ can always be made small enough by refining the division of the blade. In all the examples which will be presented in what follows ν_s was chosen equal to π while $\alpha_{i,j}$ or $\alpha_{i,j+1}$ accepted at the most a value of 6.4° (this value applied to two elements which are far from each other and their relative influence has not any practical importance). For neighbour elements $\alpha_{i,i\pm1}$ is in the order of 1° in all cases. Until now only the contribution of the vortex line which trail from the b j^{th} elements have been taken into account. In the case of curved blades also the bound vortices of all the b blades induce, in general, a velocity at the i^{th} control point. This fact is in contrast to the case of straight blades where because of symmetry these influences disappear. The influence coefficients of the bound vortices will be denoted VB_{ij} and are calculated with the help of the function G which is defined in Appendix A. According to the definitions of that Appendix and to the notations of Fig. 2, it is clear that:

$$VB_{ij} = \sum_{n=k}^{b} G(x'_i, y'_i, x''_j, y''_j, x''_{j+1}, y''_{j+1}) \tag{19}$$

while:

$$k=1 \text{ for } i\neq j \qquad\qquad k=2 \text{ for } i=j \tag{20}$$

and:

$$x'_i = x_i\cos\phi_i \tag{21a}$$

$$y'_i = x_i\sin\phi_i \tag{21b}$$

$$x''_j = r_j\cos(\phi_j + \gamma_n) \tag{22a}$$

$$y''_j = r_j\sin(\phi_j + \gamma_n) \tag{22b}$$

After all the contributions to the influence coefficients have been derived it is clear that the resultant influence coefficient VR_{ij} equals:

$$VR_{ij} = V_{ij} + C_{ij} + VB_{ij} \tag{23}$$

The induced velocity at the control point x_i will therefore be:

$$v_i = \sum_{j=1}^{m} VR_{ij}\Gamma_j \tag{24}$$

2.4 Calculating the Aerodynamic Loads

In calculating the aerodynamic loads the following assumptions, which are typical for lifting line models, are adopted:

a) The resultant velocity at all the cross sections of the blade is subsonic.

b) Any blade section is considered to work under two-dimensional flow conditions when the complete influence of the induced and axial flight velocities on the flow field is taken into account. Therefore it is possible to calculate the sectional lift, drag and moment using known two-dimensional characteristics of the airfoils. The variation of these characteristics with Mach number and Reynolds number are taken into account at each cross section, considering the local resultant velocity and chord. Such two-dimensional information can be found, for example in [8]. Theoretical support of the present assumption can be found in [9] where "lifting surface" calculations showed chordwise pressure distributions identical to two-dimensional ones inboard of the radius of maximum bound circulation. A similar experimental support is presented in [10].

c) Compressibility and viscous effects are taken into account only in the two-dimensional properties of each cross section as presented in assumption (b).

The cross sections in the present derivation are always perpendicular to the lifting line where y_{DF} and z_{DF} are cross sectional coordinates (see Fig. 3).

According to Joukowski's Theory, the lift per unit span of the blade at the control point x_i, is given by:

$$L_i = \rho W_i \Gamma_i \tag{25}$$

ρ is the air density and W_i is the magnitude of the resultant flow velocity in the blade cross section at x_i. L_i is perpendicular to the direction of W_i. In addition, according to assumption (b) L_i is also given by:

$$L_i = \frac{1}{2} \rho W_i^2 C_i a_i \alpha_i \tag{26}$$

where C_i is the local chord, α_i is the effective angle of attack and a_i is defined by:

$$a_i = \frac{C_{L_i}(R_{e_i}, M_i, \alpha_i)}{\alpha_i} \tag{27}$$

C_{L_i} is the local lift coefficient and is not necessarily a linear function of α_i. C_{L_i} is obtained from two-dimensional properties of the certain airfoil, and is a function of the local Reynolds Number R_{e_i}, the local Mach number M_i, and the effective angle of attack. The Reynolds Number is defined as:

$$R_{e_i} = \frac{W_i C_i}{\nu_a} \tag{28}$$

where ν_a is the kinematic viscosity. Mach number is defined as:

$$M_i = \frac{W_i}{V_s} \tag{29}$$

where V_s is the velocity of sound. In the present report the influence of the Mach number will be included by using the following well known equation:

$$C_{L_i} = \frac{C_{L_i}(M_i = 0)}{\sqrt{1 - M_i^2}} \tag{30}$$

which can be easily obtained from two-dimensional Prandtl-Glauert transformation.

The calculation of α_i deserves special care, as it is explained in what follows. Figure 3 shows the flow at a certain cross section of the blade. The two-dimensional properties of the blade depend on the flow field which is shown in this figure. It should be noted that because of the curvature, precone, flapping and elastic deformations, the rotational velocity, the induced velocity v_i and the axial velocity of the rotor V_C at each spanwise location should be carefully transformed to the blade cross sectional directions y_{DF}, z_{DF}. Therefore in Fig. 3 OA is mainly the projection of the rotational velocity on the y_{DF} direction, but includes small contributions due to v_i and V_C. In the same way AB is almost identical to V_C but includes small contributions due to the local

rotational speed while BC is the transformation of v_i into z_{DF} direction. OC is equal to the resultant velocity W_i. The fact that in calculating the induced velocity in subsection 2.3 assumption (a) of subsection 2.2 has been adopted while here, in applying Eq. (26), coning, flapping and deformations are taken into account, should raise the question of consistency. Any effort to remove assumption (a) in calculating the induced velocity is impractical, since it will result in an enormous complication of the theory. Since the two stages - calculating the induced velocities and calculating the two-dimensional aerodynamic characteristics - are in a way separate, it is still believed that this inconsistency is justified. The induced angle of attack, α_{ind} (see Fig. 3), equals:

$$\alpha_{ind} = \frac{v_i}{W_i} f_i \tag{31}$$

f_i is usually a number close to unity, but does not equal to unity because of the difference between the z_{HUB} and z_{DF} directions and because α_{ind} is not always a small angle. f_i is obtained from Eq. (31) as:

$$f_i = \frac{\alpha_{ind} W_i}{v_i} \tag{32}$$

From Fig. 3 it is clear that:

$$\alpha_i = \alpha_{Gi} - \alpha_{ind} \tag{33}$$

2.5 Derivation of the Complete System of Equations

Substitution of Eq. (31) into Eq. (33) and then into Eq. (26) and equating to Eq. (25), imply:

$$\Gamma_i = \frac{1}{2} W_i C_i a_i (\alpha_{Gi} - f_i \frac{v_i}{W_i}) \tag{34}$$

If the following nondimensional terms are defined

$$\tilde{W}_i = \frac{W_i}{\Omega R} ; \tilde{C}_i = \frac{C_i}{R} ; \tilde{v}_i = \frac{v_i}{R} ; \tilde{\Gamma}_i ; = \frac{\Gamma_i}{R^2} ; \tilde{VR}_{ij} = R\ VR_{ij} \tag{35}$$

then Eq. (34) becomes:

$$\frac{2}{\tilde{C}_i a_i} \tilde{\Gamma}_i + f_i \tilde{v}_i = \alpha_{Gi} \tilde{W}_i \tag{36}$$

and Eq. (24) becomes:

$$\tilde{v}_i = \sum_{j=1}^{m} \tilde{VR}_{ij} \tilde{\Gamma}_j \tag{37}$$

Substitution of Eq. (37) into Eq. (36) results in the following equation:

$$\frac{2}{\tilde{C}_i a_i f_i}\tilde{\Gamma}_i + \sum_{j=1}^{m}\tilde{VR}_{ij}\tilde{\Gamma}_j = \frac{\alpha_{Gi}\tilde{W}_i}{f_i} \qquad i=1,2,....m \qquad (38)$$

The last equation presents in fact a system of m equations which should be solved in order find the m unknowns $\Gamma_1....\Gamma_m$. Usually by using simplifying assumptions the system of Eqs. (38) becomes linear and is easily solved (see for example [5]). In the present case Eq. (38) presents a nonlinear system since all the f_i, a_i, $\tilde{W}_i$ and $\tilde{VR}_{ij}$ are functions of the induced velocities at the control points along the blade. Therefore, the system should be solved by using an iterative scheme. In all the cases which have been investigated the convergence was very fast.

The numerical procedure is very efficient and in order to find the appropriate values of V_{ij} use is made of pre-calculated tables which are stored on a computer disc. More details about the calculation procedure are given in [4].

3. Numerical Results and Discussion

Two curved blades will be investigated. One is a straight blade with a swept back tip while the second one is a blade with continuous curvature. The geometric shape of the lifting line in both cases is shown in Fig. 4. The sweep forward angle at different points along the second blade is given in the figure. The blades are plannar do not have any twist, in all the cases the pitch angle at the root equals 8°. The chord is constant and equals 0.1 L while the offset e equals zero and the root cut out is 0.2 L where L is the blade length. Two bladed rotors are investigated and in each case a comparison is made with a rotor having blades which are identical to the curved blades (also the same length) except for the fact that they are straight. Linear aerodynamics is assumed while the lift curve slope is 5.7. The distribution of the different aerodynamic variables along the blade are presented in the figures as a function of the nondimensional length α, which is the distance along the blade axis divided by its length. At the blade root α=0 while at its tip α=1. In all the cases there are eleven elements along the blades while the division is: n_i = 0.20, 0.30, 0.40, 0.50, 0.60, 0.70, 0.75, 0.80, 0.85, 0.90, 0.95, 1.00. A few examples with a more refined division gave practically identical results which shows that a satisfactory convergence is obtained by the above described division.

The results for the blades with swept tips are presented in Figs. 5a-c. In Fig. 5a the distribution of the induced velocity along the blade is presented. The regions of major influence are at the point of sweep back where the induced velocity is increased by 7% compared to the straight blade, and toward the tip where the induced velocity is reduced 7%. The lift coefficient distribution is presented in Fig. 5b. Just before the sweep back point the lift coefficient of the swept back blade is smaller than that of

the straight blade. This results from the fact that the induced velocity there is larger than in the case of straight blade. In the swept tip region there is an increase of the effective angle of attack due to the fact that the contribution of the rotational speed to the resultant velocity at the blade cross section is reduced. The decrease in the induced velocity (relative to the straight blade) toward the tip adds to the increase in the effective angle of attack which results in increasing values of the lift coefficient. In Fig. 5c the distribution of the lift force per unit length is presented. The results of the lifting line model of the present derivation are compared to those which are obtained using the "momentum-blade element" method which has been presented in [3]. Results for the "momentum-blade element" model with tip correction according to Glauert and one without this tip correction are presented. Differences between these two models exist only at the tip region. There are differences of five percent between the results of the "momentum-blade element" model and the lifting-line model at the point of sweep back while the former model yields higher results. The reason for the differences is the fact that the "momentum-blade element" theory is based on the assumption of the independence of the behaviour of any radial annulus on the behaviour of the rest of the disc (except for artificial tip corrections). On the other hand the lifting-line model includes a three-dimensional analysis where influence of neighbour cross sections is taken into account. It should also be noted that while the "momentum-blade element" theory neglects azimuthal variations in the induced velocity, the present lifting-line model includes these variations. Near the tip the lifting-line results are higher by five percent compared to the "momentum-blade element" results with tip correction.

Results for the continuously curved blade are presented in Figs. 6a-c. Because of its shape this blade is denoted "double-curved". The induced velocity distribution is presented in Fig. 6a. The trends are identical to those in the case of swept tips. The lift coefficient distribution as presented in Fig. 6b and the lift force distribution as presented in Fig. 6c, are also very similar to the distribution of the same parameters as have been presented for the case of swept tips. The main difference is of course the fact that in the case of the "double-curved" blades these parameters are continuous while in the case of swept tips a discontinuity exists at the point of sweep back.

It is interesting to note that the trends which have been presented here in the case of curved rotating blades also appear in the case of curved fixed-wings, as presented for example in [11].

4. Conclusions

A lifting line model to calculate the aerodynamic loads along a curved helicopter blade, in hovering and axial flight, has been developed. This model includes a semi-rigid wake representation. The numerical solution is very efficient and deserves very modest computation error.

The model has been applied to two different curved blades and the results were compared to the case of similar straight blades. It has been shown that curvature has an influence on the distribution of the aerodynamic properties along the blade which can be used by the rotor designer in

optimizing the rotor. The results of the present lifting line model were compared to results of a "momentum-blade element" theory which has been recently derived for curved blades by the authors of the present paper. The agreement is usually good except for increasing deviations at the tip region and regions of significant curvature. The good agreement indicates that the more important influences are those of the geometric angle of attack and the resultant velocity at each cross section. The differences result from the fact that while the "momentum-blade element" theory is based on the assumption of independence of behaviour of the disc annulus and neglecting azimuthal variations, the lifting line model, being an approximation to the three-dimensional behaviour of the rotor, does not include these assumptions.

Acknowledgements

The authors would like to thank Mrs. A. Goodman-Pinto for typing this paper and Mrs. E. Nitzan and Mrs. R. Puvlic for the preparation of the figures.

List of References

1. W.H. Weller, Experimental investigation of effects of blade tip geometry on loads and performance for an articulated rotor system, NASA TP-1303, JAN. 1979.

2. G.S. Doman, F.J. Tarzanin and J. Shaw, Investigation of aeroelastically adaptive rotors, USAAMRDL TR-77-3, MAY 1977.

3. A. Rosen and O. Rand, The aeroelastic behavior of curved helicopter blades in hovering and axial flight, TAE Report 481, Technion-Israel Institute of Technology, Dept. of Aeronautical Engineering, Haifa, Israel, March 1982. Condensed version of this report, having the same title, appears in the Proceedings of the 24th Israel Annual Conference on Aviation and Astronautics, February 17-18, 1982, pp. 129-139. It has also been submitted for publication.

4. O. Rand and A. Rosen, Prediction of the aerodynamic loads on helicopter blades in hovering and axial flight using lifting line theory, Proceedings of the 24th Israel Annual Conference on Aviation and Astronautics, February 17-18, 1982, pp. 117-128. It has also been submitted for publication.

5. V.E. Baskin, L.S. Vil'dgrube, Ye.S. Vozhdayev and G.I. Maykapar, Theory of the lifting airscrew, NASA TT F-823, FEB. 1976.

6. Th. van Holten, On the validity of lifting line concepts in rotor analysis, Vertica, Vol. 1, 1977, pp. 239-254.

7. S.E. Windnall, The structure and dynamics of vortex filaments, Annual Review of Fluid Dynamics, Vol. 7, pp. 141-165, 1975.

8. I.H. Abbott and A.E. Von Doenhoff, Theory of wing sections, Dover Publications, Inc., New York.

9. K.R. Shenoy and R.B. Gray, Iterative lifting surface method for thick bladed hovering helicopter rotors, Journal of Aircraft, Vol. 18, No. 6, June 1981.

10. J. Scheiman and H.L. Kelley, Comparison of flight-measured helicopter rotor-blade chordwise pressure distributions with static two-dimensional airfoil characteristics, NASA TN D-3936, MAY 1967.

11. J. Ashenberg and D. Weihs, Curved lifting-line theory for thin planar wings, Proceedings of the 24th Israel Annual Conference on Aviation and Astronautics, February 17-18, 1982, pp. 208-212.

Appendix A - The Function G

The function G is explained in Fig. (A-1). A straight vortex filament whose circulation equals unity (the positive direction of the circulation is shown in the figure) is stretched from point (x_2, y_2) to point (x_3, y_3). The velocity induced by this vortex filament in the -z direction, at the point (x_1, y_1) is given by the function $G(x_1, y_1, x_2, y_2, x_3, y_3)$. According to Biot-Savart's law and using the notation of Fig. (A-1) it is clear that:

$$G(x_1, y_1, x_2, y_2, x_3, y_3) = \frac{1}{4\pi d} (\cos\theta_1 + \cos\theta_2) \qquad (A-1)$$

A computer function has been prepared, which calculates the value of G as a function of the six numbers in the parentheses.

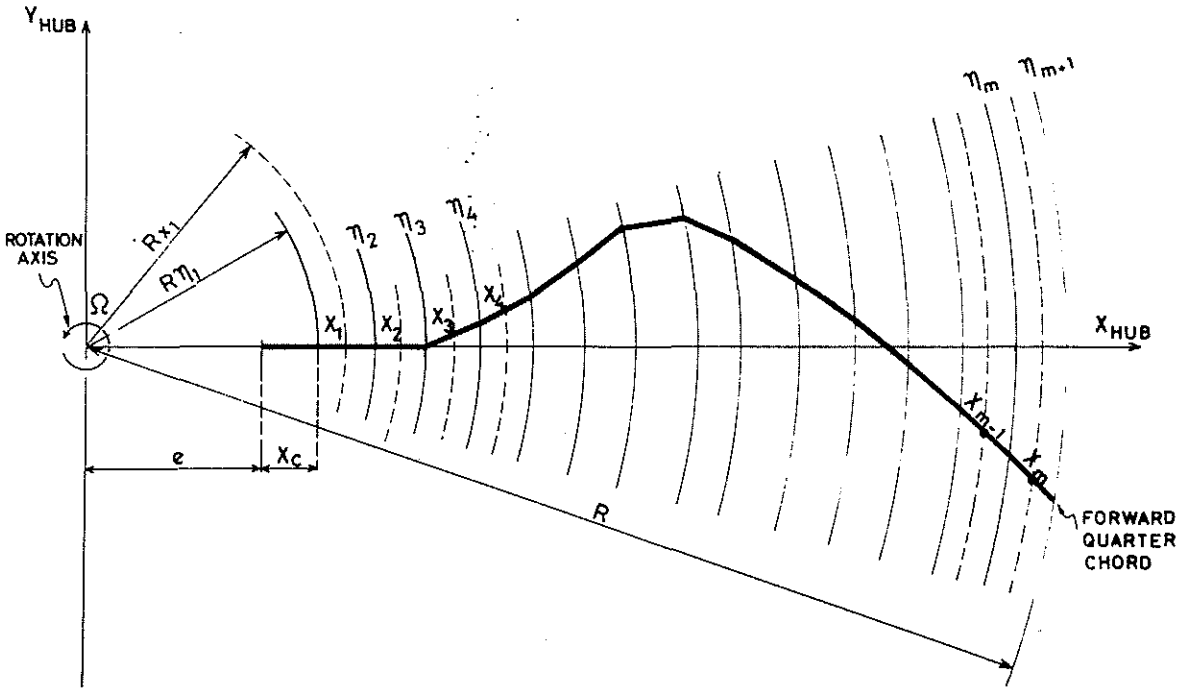

FIGURE 1: PROJECTION OF BLADE GEOMETRY ON x_{HUB} - y_{HUB} PLAN.

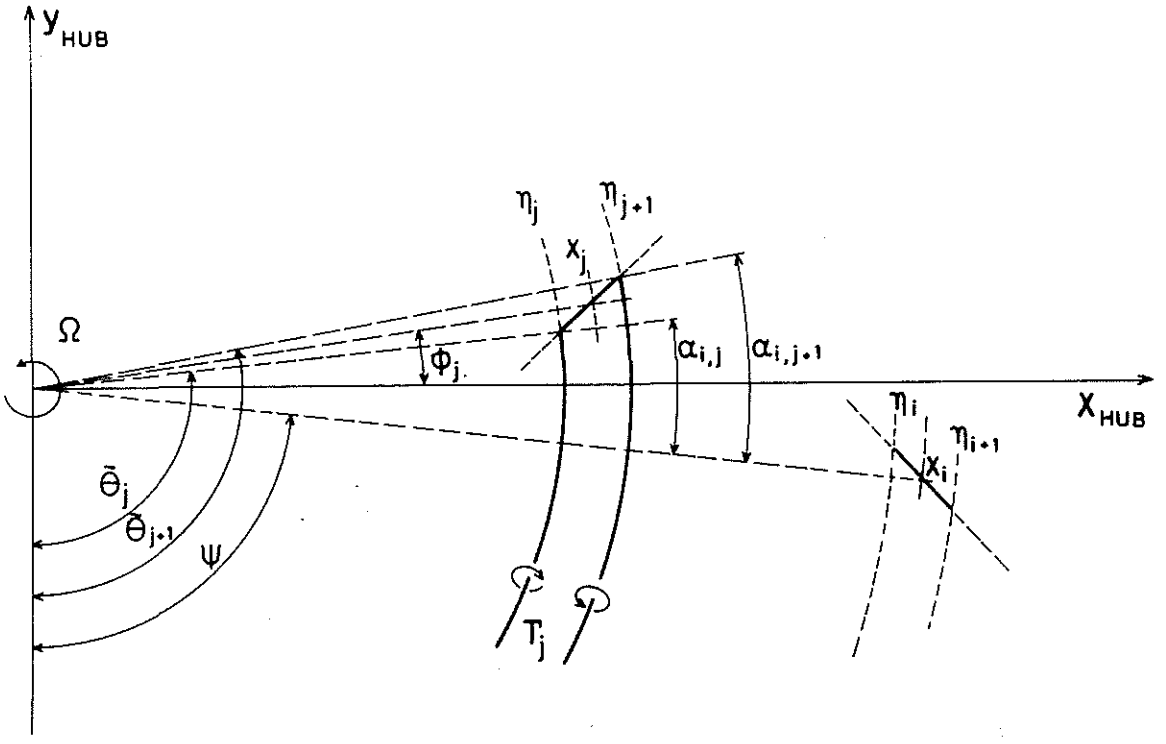

FIGURE 2: DESCRIPTION OF THE i^{th} AND j^{th} ELEMENTS.

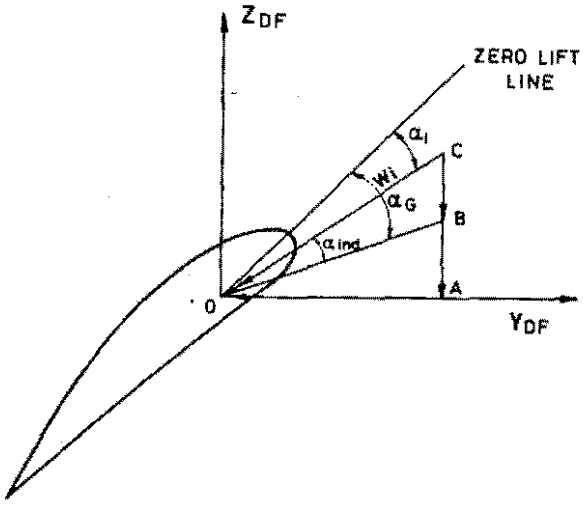

FIGURE 3: FLOW FIELD AT THE BLADE CROSS SECTION.

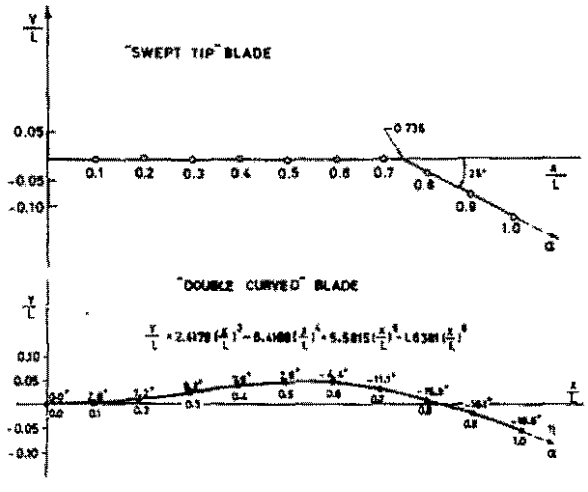

FIGURE 4: GEOMETRY OF THE BLADES.

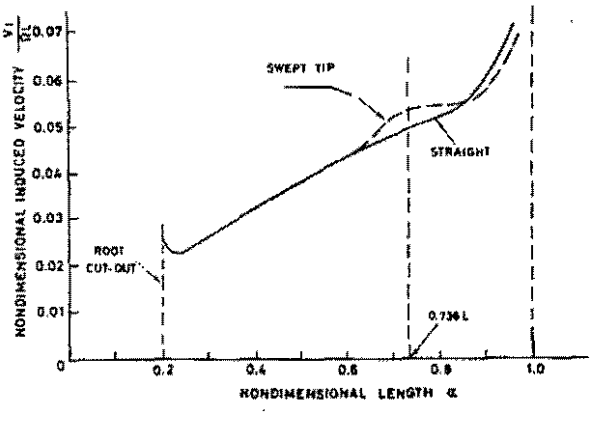

FIGURE 5a: THE INDUCED VELOCITY DISTRUBTION ALONG THE "SWEPT TIP" BLADE.

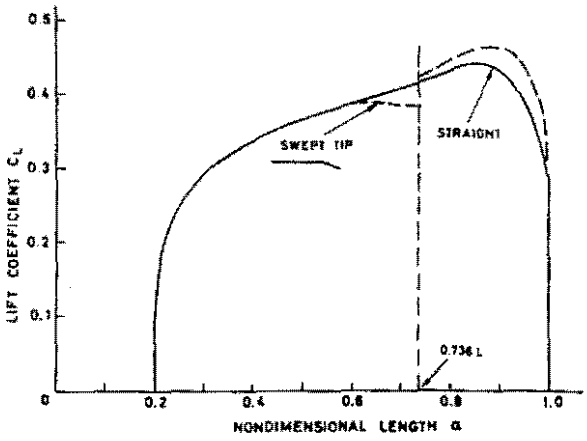

FIGURE 5b: THE LIFT COEFFICIENT DISTRIBUTION ALONG THE "SWEPT TIP" BLADE.

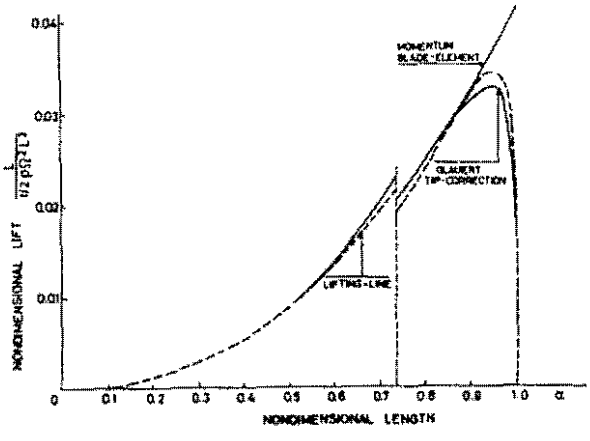

FIGURE 5c: THE LIFT PER UNIT LENGTH DISTRIBUTION ALONG THE "SWEPT TIP" BLADE.

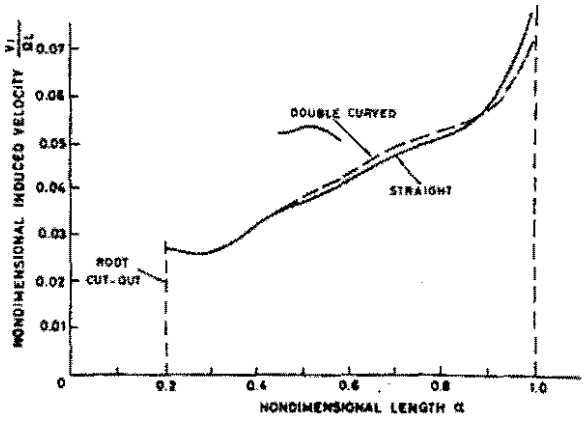

FIGURE 6a: THE INDUCED VELOCITY DISTRIBUTION ALONG THE "DOUBLE CURVED" BLADE.

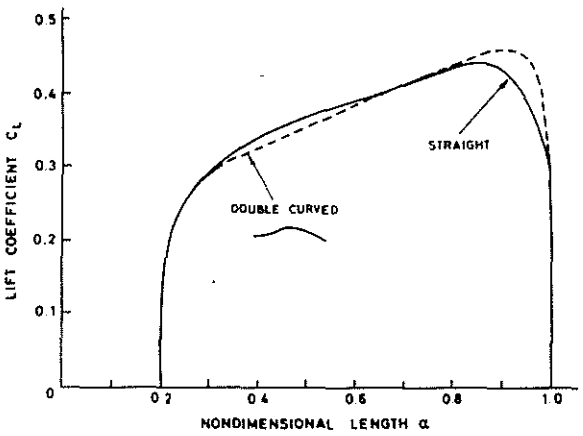

FIGURE 6b: THE LIFT COEFFICIENT DISTRIBUTION ALONG THE "DOUBLE CURVED" BLADE.

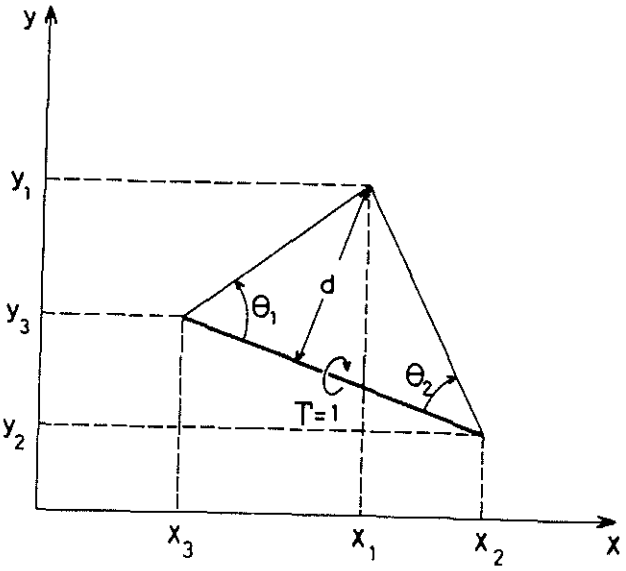

FIGURE (A-1) - THE MODEL ASSOCIATED WITH THE FUNCTION G.

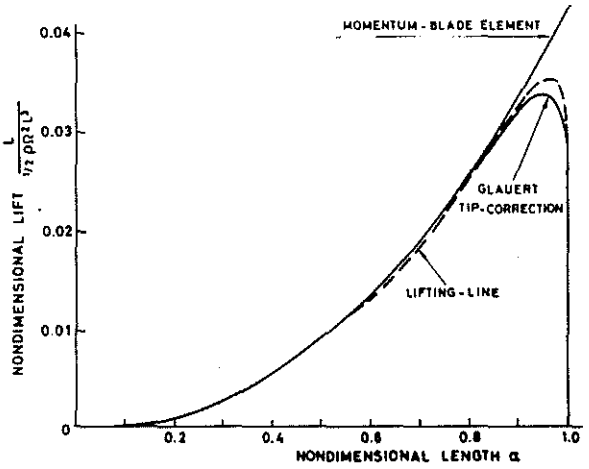

FIGURE 6c: THE LIFT PER UNIT LENGTH DISTRIBUTION ALONG "DOUBLE CURVED" BLADE.